A molecular simulation approach to the prediction of the morphology of self-assembled nanoparticles in diblock copolymers†

Paola Posocco,[a] Zbyšek Posel,[b] Maurizio Fermeglia,[a] Martin Lísal[bc] and Sabrina Pricl*[a]

Received 22nd May 2010, Accepted 14th July 2010
DOI: 10.1039/c0jm01561j

Mixing microphase-separating diblock copolymers and nanoparticles can lead to the self-assembly of organic/inorganic hybrid materials that are spatially organized on the nanometre scale. Controlling particle location and patterns within the polymeric matrix domains remains, however, an unmet need. Computer simulation of such systems constitutes an interesting challenge since an appropriate technique would require the capturing of both the formation of the diblock mesophases and the copolymer–particle and particle–particle interactions, which can affect the ultimate structure of the material. In this work we discuss the application of *Dissipative Particle Dynamics* (DPD) to the study of the distribution of nanoparticles with different degree of functionality and volume fraction in a lamellar microsegregated copolymer template. The DPD parameters of the systems were calculated according to a multi-step modelling approach, *i.e.*, from lower scale (atomistic) simulations. The results show that positioning and ordering of the nanoparticles, as well as the dimensions of the block domains depend on covering extent and volume fraction, in full agreement with experiments. The overall results provide molecular-level information for the rational, *a priori* design of new polymer–particle nanocomposites with *ad hoc*, tailored properties.

Introduction

According to the International Union for Pure and Applied Chemistry (IUPAC),[1] a composite material is defined as "a multicomponent material comprising multiple different (non-gaseous) phase domains in which at least one type of phase domain is in a continuous phase". IUPAC also extends its definition to nanocomposite materials as those composites "in which at least one of the phases has at least one dimension of the order of nanometres". Based on these definitions, a plethora of systems can be classified among these materials, the dispersions of nanosized objects of different nature – ranging from metal particles to carbon nanotubes to layered minerals in continuous/polymeric phases – being prime examples.

Notwithstanding the mixing of nanoparticles of different shapes and sizes with polymers to generate polymer nanocomposites (PNCs) has been practised for decades,[2] a large-scale production and commercialization of these new materials is still hindered by the absence of cost-effective methods for controlling the dispersion of the nanoparticles in the polymeric hosts. Indeed, random arrangements of the nanoparticles within the macromolecular matrix will not provide optimized mechanical, electrical, thermal, optical or barrier performance for many potential high-technology applications, such as dielectric underfills for electronic packaging, printed flexible electronics, engineered aerospace structural components, reconfigurable conductive adhesives, and optical gratings just to mention a few.

Recently, however, it has been suggested that block copolymers, with their rich diversity of morphologies arising from their microphase separation properties can provide an effective means to control the particle location and dispersion.[3] Indeed, the microphase separation of the block copolymers could be harnessed to promote the ordering of the nanoparticles and thereby create highly organized hybrid materials. Such spatially regular composites can have high impact in nanotechnology, exploiting their exceptional properties. The direct self-assembly of the copolymer and particles could also be exploited to create materials inspired by nature. For instance, one can envision creating shell-like structures, where layers of polymers alternate with layers of inorganic species.

A few experimental approaches have been proposed so far for the incorporation of nanoparticles selectively into the preferred domain of block copolymers to originate 2D and 3D spatial distribution of nanoparticles in polymeric matrices. In particular, a few years ago Chiu and co-workers devised an apt procedure to incorporate gold nanoparticles and control their location within a poly(styrene-*b*-2-vinylpyridine) (PS-PVP) diblock copolymer matrix by changing the surface chemistry of the particles.[4] In detail, to localize the gold nanoparticles within either of the two block domains, the particle surface must be made "neutral" with respect to that domain. In other terms, the particle must be grafted with either PS or PVP homopolymers. On the other hand, if particles should be located at the block interfaces, they must be grafted by a mixture of PS and PVP homopolymers.[4b] Alternatively, however, as PVP interacts more favourably with gold than PS, a low degree of PS coverage alone can be

[a]*Molecular Simulations Engineering (MOSE) Laboratory, Department of Materials and Natural Resources (DMNR), University of Trieste, Piazzale Europa 1, 34127 Trieste, Italy. E-mail: SABRINA.PRICL@dicamp.units.it*
[b]*Department of Physics, Faculty of Science, J. E. Purkinje University, 400 96 Ústí nad Labem, Czech Republic*
[c]*E. Hála Laboratory of Thermodynamics, Institute of Chemical Process Fundamentals of the ASCR, v. v. i, 165 02 Prague 6-Suchdol, Czech Republic*
† This paper is part of a *Journal of Materials Chemistry* themed issue on Modelling of Materials. Guest editors: Julian Gale and Mark Wilson.

employed. In fact, this exposes a substantial part of the bare Au particle to the surrounding medium and leads to favorable interactions of the few grafted PS chains with the PS block and favorable interactions of the bare Au with the PVP block, with the ultimate result of leading to domain interface particle segregation. In addition, in the context of nanoparticle dispersion, a recent study based on accurate computational techniques confirmed that bare metal nanoparticles with very high surface and cleavage energy compared to the surface tension/cleavage energy of the diblock copolymer lead to aggregation unless modified for compatibilization. Surface modification of the nanoparticle reduces the cohesive energy (cleavage free energy) between nanoparticle agglomerates to values similar to the diblock copolymer domains and improves dispersion.[5]

The procedure described above is of general importance and widely applicable to other block copolymer and nanoparticle systems and, since the properties of the final nanocomposites strongly depend on the nature of the dispersion as well as on ordering of particles in the polymer, tailoring nanoparticles into arrays in an ordered polymer phase provides exciting new possibilities on the material front. Accordingly, a detailed understanding of the effects of the molecular properties of block copolymers and nanoparticles on the self-assembled structures of the nanocomposites is essential to develop strategies to fabricate novel composites with unique and functional characteristics.

Developing such an understanding is hampered by the fact that the number of parameters controlling the behaviour of the system is large: the observed microstructures clearly depend on the size, shape and volume fraction of the particles, the composition of the polymers, and the interaction energies between the different species.

Under this perspective, in this work, we present an approach for determining the equilibrium morphologies for mixtures of diblock copolymer melts and solid nanoparticles based on a multi-step molecular modeling methodology. In particular, we provide a complete description of our modeling ansatz and focus on gold nanoparticles interspersed in a PS-PVP matrix with a microsegregated lamellar morphology as a proof-of-concept. One motivation for the choice of this particular system undoubtedly resides in the wide availability of experimental evidences, against which the modeling results can be validated. However, another and perhaps more important reason can be found in the potential, practical applications of these specific PNCs. Indeed, when the PS-grafted gold nanoparticles can be located in the middle of the corresponding compatible block domain of the PS-PVP diblock copolymer, they can give rise to nanowire-like structures that extend throughout the material. Such materials could constitute a sort of nanoelectrode array, which could be utilized to fabricate, *e.g.*, organized nanodevices. On the other hand, when the particles are forced to segregate at the interfaces instead of the centers of the lamellae, if the copolymer matrix was to be dissolved from the system, the remaining inorganic phase could give origin to a nanoporous material, with a regular arrangement of uniform pores, which could find applications, for instance, in separation or catalytic processes.

Results and discussion

The location of nanoparticles within a block copolymer matrix is primarily influenced by the compatibility of the nanoparticles with each constituent of the block copolymer microstructure. Therefore, surface modification of the nanoparticles is required not only to stabilize them against aggregation but also to tune their interactions with each block copolymer domain.

A simple strategy to control the location of polymer-coated gold nanoparticles within PS-PVP block copolymer domains is the variation of a single parameter: the surface coverage of the nanoparticles by a homopolymer PS (or PVP) ligand. Indeed, it has been verified experimentally that, as the areal chain density Σ of the PS chains on the nanoparticle (*i.e.*, the number of PS chains grafted on the nanoparticle per nm^2) decreases, a transition from the case where the nanoparticles are located in the PS domain to the case where the nanoparticles are located at the PS-PVP interface is observed.[4]

To systematically investigate this aspect, the nanoparticle location within the block copolymer template was studied as a function of the polystyrene (PS) coverage surface through a library of four different coverage percentages represented by four different surface architectures: PS_1Au_{11}, PS_2Au_{10}, PS_3Au_9, PS_4Au_8. Thus, for instance, a PS_1Au_{11} model describes an icosahedron nanoparticle where 1 bead on the surface is of type PS and the remaining 11 beads are of type Au. The central bead is always of type Au.

Effect of PS grafting density for nanoparticle volume fraction $\phi_p = 0.05$ and 0.1

Fig. 1a shows the self-assembled lamellar phase where the particles with substantial coverage of PS (PS_4Au_8) at a constant nanoparticle volume fraction $\phi_p = 0.05$ collect in the center of the PS-block region, forming almost continuous nanosheets. This is an expected result since, when the Au nanoparticles are made "neutral" towards the PS block (*i.e.*, when the unfavorable interactions between Au and PS are shielded by the presence of the grafted PS chains), the nanoparticles lower their enthalpy by segregating into the corresponding domain of the block copolymer. Furthermore, by concentrating the particles near the center of the compatible domain where the polymer ends are located, the chains can accommodate the particles by moving apart rather than by stretching. Localizing particles near the center of the compatible domain thus sacrifices some translational entropy of the particles but avoids an even larger chain stretching penalty incurred by distributing the particles throughout the domain.

As the PS grafting density drastically decreases at constant $\phi_p = 0.05$, virtually all nanoparticles locate at the interface between the PS and PVP block domains, as shown in Fig. 1d (PS_1Au_{11}). PS-Au nanoparticles with intermediate coverage stay bound to the interface for PS_2Au_{10}, as highlighted in Fig. 1c, while the nanoparticles are progressively directed to the PS domain at a coverage corresponding to PS_3Au_9 (Fig. 1b).

The decrease of PS grafting density thus induces a transition of nanoparticle location from the PS domain to the PS-PVP interface. A rationale for this behavior can be formulated as follows. Because PVP segments are preferentially attracted to the bare gold particle surface over PS segments, attaching short PS chains to the nanoparticle at a low Σ values exposes bare Au to the surrounding medium and leads to favorable interactions of the grafted PS chains with the PS block and

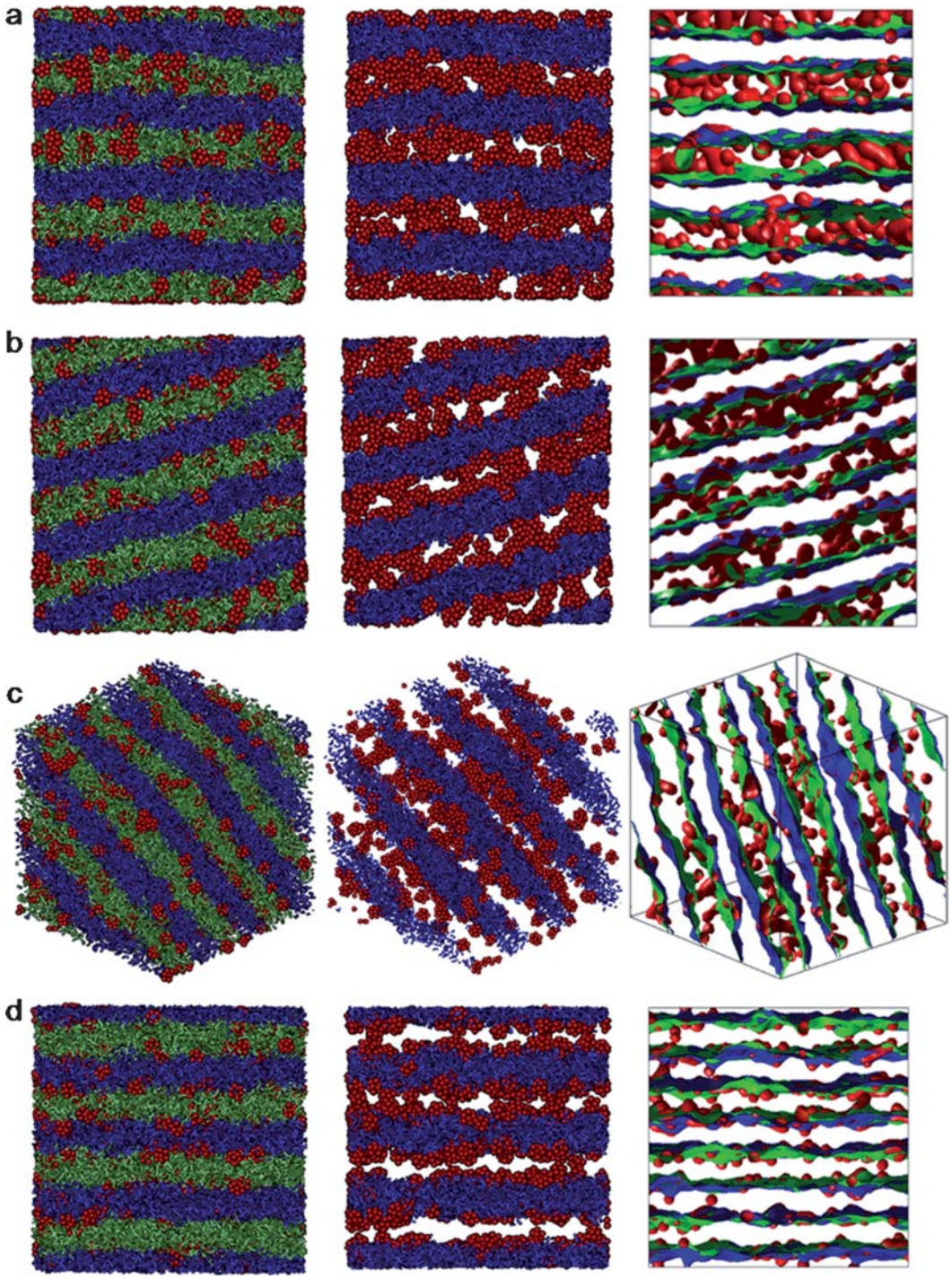

Fig. 1 Left and middle columns: snapshots of the simulated PNC structures corresponding to a volume fraction of $\phi_p = 0.05$ and to different nanoparticle coverage: a, PS_4Au_8; b, PS_3Au_9; c, PS_2Au_{10}; d, PS_1Au_{11}. The PS domain was omitted from the snapshots in the central column for clarity. Right column: isosurface visualization of each component (PS, PVP and nanoparticles): PS-type beads (green), PVP-type beads (blue), Au nanoparticle beads (red).

favorable interactions of the bare Au with the PVP block. As a result, the strong adsorption of such partially PS-coated nanoparticles to the interface occurs. In other words, the PS-Au nanoparticles characterized by a low Σ segregate to the interface due to the inability of the few grafted chains to screen the favourable interaction between the PVP block chains and the exposed Au surface. Importantly, the segregation of PS-coated nanoparticles at the PS-PVP interface is observed over a range of Σ values.

To quantitatively reinforce the qualitative impressions yielded by Fig. 1, Fig. 2 shows the plots of the density distributions of the nanoparticles, and the PS and PVP components of the copolymer matrix in the direction perpendicular to the lamellae. The first diagram (Fig. 2a) clearly shows the occurrence of a single peak in

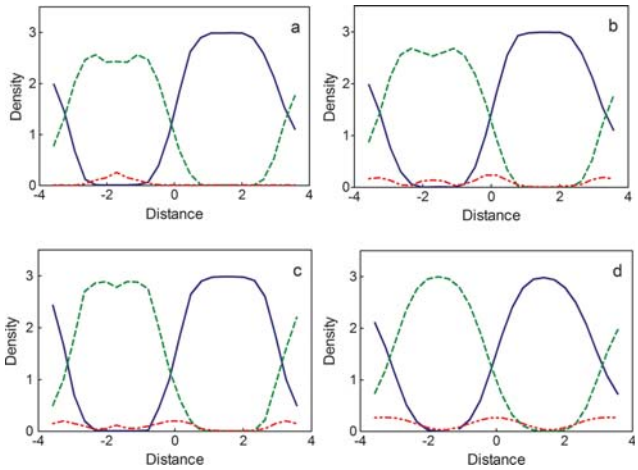

Fig. 2 One-dimensional density profiles of the simulated PNCs with lamellar morphology and particles at $\phi_p = 0.05$ in the direction perpendicular to the lamellae. Nanoparticle coverage architecture: a, PS_4Au_8; b, PS_3Au_9; c, PS_2Au_{10}, d, PS_1Au_{11}: PS (green), PVP (blue), Au (red).

the particle density distribution at the center of the PS domain when particles have a relatively high grafting coverage, and thus the unfavourable interaction between the PS ligands of the particle surface and the PVP domain is dominant.

As the grafting density decreases, the height of the peak due to the location of the particles at the center of the PS domain reduces, whilst the appearance of two further peaks, related to the particles bound at the PS-PVP interface, becomes manifest. Upon further decrease in Au-nanoparticle surface coverage, the particles are almost entirely bound to the PS-PVP domain interface; accordingly, the heights of the corresponding peaks increase while the peak at the center of the PS domain disappears.

The trend in the dramatic change of the particle location from the center of PS domain to the interface is preserved when the particle concentration is increased up to $\phi_p = 0.1$. The DPD simulation snapshots and isosurface visualization of the PS-PVP

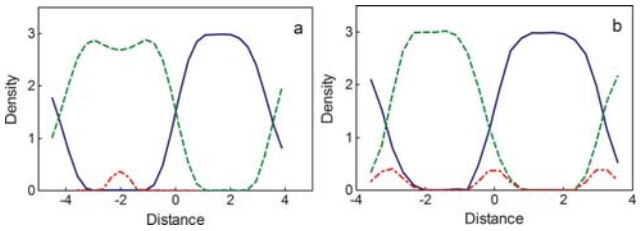

Fig. 4 One-dimensional density profiles of the simulated PNCs with lamellar morphology and particles at $\phi_p = 0.1$ in the direction perpendicular to the lamellae. Nanoparticle coverage architecture: a, PS_4Au_8; b, PS_1Au_{11}: PS (green), PVP (blue), Au (red).

block copolymer containing PS-grafted gold nanoparticles at constant $\phi_p = 0.1$ and at the two extreme degree of coverage considered are shown in Fig. 3 as an example. When the value of Σ is high, the particles are mostly located within the PS domain, while most gold particles with low Σ are segregated to the PS-PVP interface. The corresponding diagrams of the density distribution of the nanoparticles and the PS and PVP components of the copolymer matrix in the direction perpendicular to the lamellae, as shown in Fig. 4, nicely reflect the transition of particle location in the PS-PVP template at $\phi_p = 0.1$.

Importantly, however, at both gold particle volume fractions $\phi_p = 0.05$ and 0.1, the lamellar morphology of the copolymer matrix is preserved.

Estimation of the interlamellar spacing for PS_4Au_8 at $\phi_p = 0.05$ and 0.1

Focussing now the attention to the nanoparticles with high values of Σ, a semi-quantitative rationale for the dependence of the nanoparticle degree of coverage on the constitution of the "lamellar-loaded" and "lamellar-unloaded" domains can be formulated by considering the change in dimensions of the copolymer block domains as a function of ϕ_p. Due to the covalent nature of the bonds between the two blocks in the

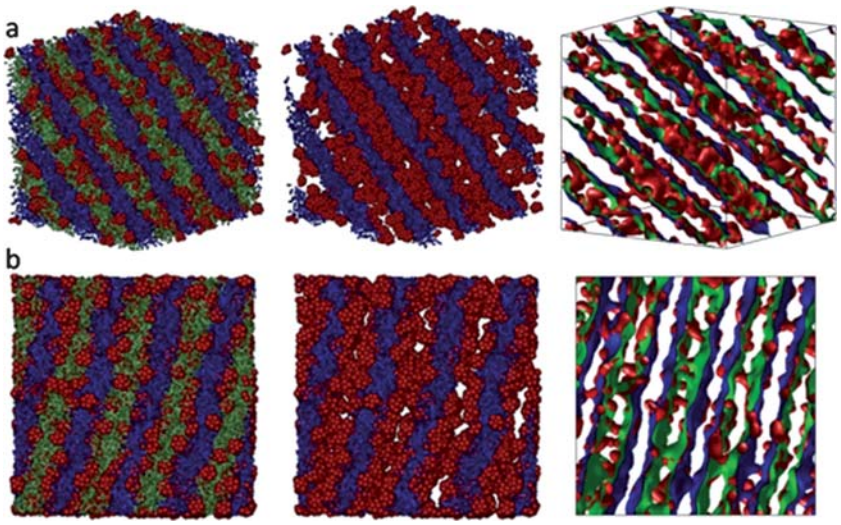

Fig. 3 Left and middle columns: snapshots of the simulated PNC structures corresponding to a volume fraction of $\phi_p = 0.1$ and to different nanoparticle coverage: a, PS_4Au_8; b, PS_1Au_{11}. The PS domain was omitted from the snapshots in the central column for clarity. Right column: isosurface visualization of each component (PS, PVP and nanoparticles): PS-type beads (green), PVP-type beads (blue), Au nanoparticle beads (red).

copolymer, adjoining blocks must preserve an equal interfacial area per junction, σ, should the lamellar microstructure be preserved. The resulting coupling of dimensional changes of the respective block domains renders the mixing process dependent on the architecture of all constituting blocks. For systems such as those considered in this work, the change in domain dimensions can be estimated invoking a free energy argument originally formulated by Ausserré *et al.*,[6] and briefly summarized below.

For a given diblock copolymer AB with a microsegregated lamellar morphology and volume fraction $\phi_{AB} = N_A/(N_A + N_B)$ of the particle-filled (A) domain, the dependence of the layer dimension on the particle volume fraction ϕ_p can be expressed as:

$$\frac{H_{p,0}}{H_0} = \Lambda^{-1/3}(\phi_{AB}, \phi_p)\frac{1}{1-\phi_p} \quad (1)$$

$$\frac{h^A_{p,0}}{h^A_0} = \Lambda^{-1/3}(\phi_{AB}, \phi_p)\left(1 + \frac{1}{\phi_{AB}}\frac{\phi_p}{1-\phi_p}\right) \quad (2)$$

$$\frac{h^B_{p,0}}{h^B_0} = \Lambda^{-1/3}(\phi_{AB}, \phi_p) \quad (3)$$

in which:

$$\Lambda(\phi_{AB}, \phi_p) = \frac{\phi_{AB} + (1-\phi_{AB})\phi_p^2}{\phi_{AB}(1-\phi_p)^2} \quad (4)$$

In the above equations, $H_{p,0}$ and H_0 denote the equilibrium lamellar spacing, and $h^i_{p,0}$ and h^i_0 are the segment length of the ith block in the particle-filled and neat block copolymer, respectively. The change in the interfacial area per junction σ upon increasing ϕ_p can be obtained from eqn (1)–(3) as:

$$\sigma_{p,0} = \frac{2NB^3}{H_{p,0}} = \sigma_0 \Lambda^{1/3}(\phi_{AB}, \phi_p) \quad (5)$$

where $\sigma_0 = 2NB^3/H_0$ denotes the equilibrium interfacial area per junction of the unfilled copolymer, N is the total degree of polymerization, and b is an average monomer size.

According to this model, the block-selective dispersion of nanoparticles within a diblock copolymer is predicted to induce both axial and lateral swelling of the corresponding lamellar-loaded domains. Due to the constraint of equal σ, the lateral swelling induces an axial compression of the lamellar-unloaded polymer domains.

The behavior predicted by the theory discussed above is indeed obeyed by the systems in which the nanoparticles are characterized by the higher values of the areal chain density Σ, as can be qualitatively inferred by comparing Fig. 2a and 4a. A quantification of the swelling/compression of the PS/PVP domains is yielded by the comparison of the values obtained from the application of eqn (1)–(3) to the systems with nanoparticle architecture PS_4Au_8 and $\phi_p = 0.05$ and 0.1 with the information extracted from the relevant DPD simulations, as shown in Table 1.

Table 1 Values of the ratios of the segment length of the ith block in the particle-filled and neat block copolymer for the systems with gold nanoparticle architecture PS_4Au_8 and volume fraction 0.05 and 0.1 as obtained from the application of eqn (1)–(3) (th) and from the DPD simulations (sim)

$(h^{PS}_{p,0}/h^{PS}_0)_{th}$	$(h^{PS}_{p,0}/h^{PS}_0)_{sim}$	$(h^{PVP}_{p,0}/h^{PVP}_0)_{th}$	$(h^{PVP}_{p,0}/h^{PVP}_0)_{sim}$
1.07	1.10	0.97	0.99
1.14	1.15	0.93	0.92

Effect of PS grafting density for nanoparticle volume fraction $\phi_p = 0.2$

As ϕ_p is increased to 0.2, the results show that also in this case the lamellar mesophase of the neat block copolymer is preserved and that the nanoparticles are localized in the PS domains of the block copolymer. However, large regions of aggregated nanoparticles are also present at this nanoparticle loading, indicating a coexistence between a macrophase higly enriched in nanoparticles, and a lamellar mesophase with a substantially lower nanoparticle concentration, as illustrated in Fig. 5a for the PS_4Au_8 nanoparticles. The predicted behaviour is fully consistent with the experimental evidence of Kim *et al.*,[7] shown for comparison in Fig. 5b.

The behavior of the particles with high Σ values as a function of ϕ_p is easily understood by considering that, when the particle concentration is increased, the distribution of the PS–Au particles around the center of the PS domain becomes narrower. In our case, particles simply packed more densely around the center of the PS domain, as evidenced by the corresponding density profiles (see Fig. 2 and 4). At higher values of ϕ_p, the particle dispersion within the PS domain becomes progressively more unfavourable as the PS chains must stretch farther to accommodate more particles. This increase in stretching penalty cannot be offset by particle translation entropy, and thus the particles are prevented from spreading throughout the PS domains. To accommodate still higher ϕ_p without incurring in unexceedingly large stretching penalty, more particles localize near the center of the compatible PS domain. As a result, the width of the particle distribution in the PS domain profile narrows as the filling fraction increases. As particle loading increases further, the local concentration gradient of nanoparticles increases the interfacial

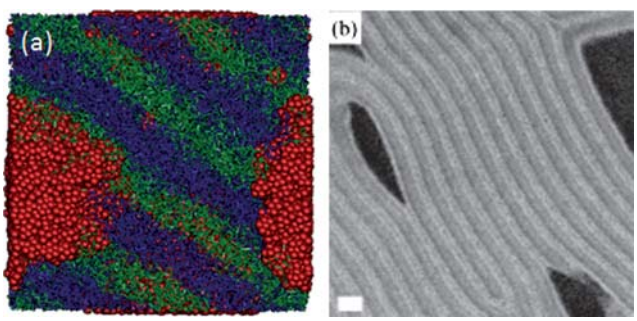

Fig. 5 a: Snapshot of the simulated PNC structure corresponding to the PS_4Au_8 nanoparticle coverage and volume fraction $\phi_p = 0.20$: PS-type beads (green), PVP-type beads (blue), Au nanoparticle beads (red). b: cross-sectional TEM image showing the macrophase separation of gold nanoparticles in symmetric PS-*b*-PVP block copolymers (reproduced from ref. 7 with permission of the American Chemical Society).

roughness between the two domains, inducing distortion in the morphology. Finally, above a threshold volume fraction of the nanoparticles, the excess particles cannot assemble in the preferred domain, and the system undergoes a macrophase separation of particles coexisting with an ordered polymer/nanoparticle phase.

Kim and co-workers[7,8] also verified the formation of a stable bicontinuous phase by increasing the volume fraction of low Σ PS–Au nanoparticles. In our case, the simulation always yields a lamellar morphology. This seeming discrepancy between theory and experiment can be easily understood by considering that the limit for the lamellar-bicontinuous transition increases with decreasing the polymer molecular weight. Since the copolymer simulated in this work has a molecular weight somewhat lower than that experimentally employed by Kim in his study,[7,8] the formation of a bicontinuous phase in our conditions is expected to take place at higher particle volume fractions. Accordingly, the transition between lamellar and bicontinuous morphology is correctly not detected.

At the same volume fraction $\phi_p = 0.2$, when Σ decreases, the overall system morphology reverts to a regularly ordered lamellar geometry (see Fig. 6). However, we noticed that the PS domain thickness progressively decreases with decreasing Σ whilst the PVP domain thickness increases correspondingly. Thus, in passing from the systems with nanoparticle architecture PS_3Au_9 to that with architecture PS_1Au_{11} the normalized PS domain spacing $h_{p,0}^{PS}/h_0^{PS}$ changes from 1.25 to 1.10, while the corresponding quantity for PVP, $h_{p,0}^{PVP}/h_0^{PVP}$, increases from 0.99 to 1.05. These predictions are in harmony with analogous results obtained from previous computational studies based on discontinuous molecular dynamics simulations performed by Hall and collaborators.[9] A sensible explanation for this behavior can be traced to the fact that the segregation of the nanoparticles to the block copolymer interface leads to a decrease in interfacial tension between the two blocks of the copolymer, consequently causing a decrease in the domain spacing. Since the blocks of copolymer stretch and lose entropy in order to decrease the interfacial area and, thus, the total energy of the interface between the two blocks, segregation of nanoparticles to the interface, which leads to a decrease in interfacial tension, allows the stretched blocks to relax and leads to a corresponding decrease in the domain spacing.

Summarizing the effect of the areal chain density at fixed volume fraction 0.2, we can say that, as Σ increases, the variation of the size of the PS domain is almost coincident with the variation of the periodic spacing, indicating the swelling of the PS domains as responsible for most of the variation in the overall periodic spacing. The size of the PVP domain is generally less than it would be if the nanoparticle were removed. The contraction of the PVP domain can be related to the fact that the nanoparticles have a higher concentration at the interface than in the PVP domain. Nanoparticles at the interface force apart copolymer chains, effectively stretching the lamellar sheet laterally (*i.e.*, parallel to the lamellar interface) and creating voids within the PVP domain. The PVP domain then contracts perpendicularly to the interface to maintain a constant density in the system if other nanoparticles do not fill these voids. The concentration of the nanoparticles at the interface decreases as Σ increases; consequently, the contraction of the PVP domain becomes smaller.

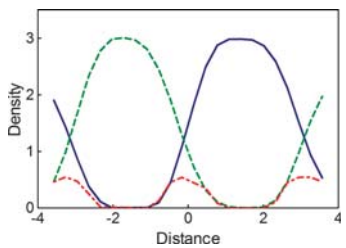

Fig. 6 One-dimensional density profiles of the simulated PNC structure corresponding to a volume fraction of $\phi_p = 0.2$ and a nanoparticle coverage PS_1Au_{11} in the direction perpendicular to the lamellae: PS (green), PVP (blue), Au (red).

Conclusions

This work represents an application of a multi-step molecular modeling procedure to the prediction of the distribution of functionalized nanoparticles in a diblock copolymer matrix as a function of some fundamental system parameters. In particular, the proposed computational methodology predicts the effects of particle volume fraction (ϕ_p) and surface chemistry (Σ) on lamellar structure in qualitative agreement with the relevant experimental evidences.

Applying the simulation *ansatz* to a real system of practical interest, *i.e.*, gold nanoparticles functionalized by short poly(styrene) chain interspersed in a lamellar microsegregated poly(styrene-*b*-2-vinylpyridine) diblock copolymer matrix, the mesoscopic simulations results revealed that, for nanoparticles characterized by a high value of the areal chain density Σ, the effects of the volume fraction of the nanoparticles dispersed in either domains of the block copolymer can be summarized as follows. At low ϕ_p values, the nanoparticles are well dispersed and organized in the preferred domain of the block copolymer. As the particle loading increases, the local concentration gradient of nanoparticles increases the interfacial roughness between the two domains, resulting in a distortion of the lamellar morphology. Above a given threshold ϕ_p value of nanoparticles, the excess particles can no longer assemble in the preferred domain, and the system undergoes a macrophase separation of particles coexisting with an ordered polymer/nanoparticle phase. Interestingly, again at high Σ values and intermediate ϕ_p, the simulation is able to reproduce the swelling of the particle-loaded lamellar domains and the consequent compression of the alternative particle-empty polymer domains.

As concerns the effect of a Σ variation at constant ϕ_p, the segregation of the nanoparticles toward the block domain interface is correctly predicted, together with the corresponding variation of the single domain spacings.

Our understanding of the property–morphology correlations in these systems is still arguably at its infancy, but is progressing rapidly, identifying the relative contribution of interface properties, nanoparticle distributions, and nanoparticle–polymer interactions to the final property suite. The addition of increased morphology control and its associated property implications, including anisotropy in physical characteristics on the

macroscale, will broaden the potential impact of PNCs beyond the current commodity applications.

Of the numerous challenges to achieve this goal, two stand out with respect to their substantial impact and pervasiveness: phase behavior and nanoparticle interface modification. Theory, modeling and experimental validation of the phase behavior underpin all concepts to add order to the random assembly. Quantification of the interactions and their impact on the structure drives selection of NP modification. The development of a plurality of approaches to control nanoparticle order will provide solutions to the future manufacturing needs.

Computational methods

Simulation theory and models

DPD theory. In 1992, Hoogerbrugge and Koelman introduced a mesoscale technique to simulate the hydrodynamic behavior of soft matter called *Dissipative Particle Dynamics* (DPD).[10] Similar to molecular dynamics (MD) or Brownian dynamics (BD), DPD is a particle-based method. However, what essentially differentiates the DPD method from the above-mentioned simulation techniques is that (i) in DPD a number of atoms are coarse-grained to a fluid element, thereafter called a DPD particle, (ii) the DPD particles interact with each other *via* soft potentials, thereby allowing for time scale of simulations substantially larger than in MD, and (iii) the use of pair-wise dissipative and random forces, in addition to the conservative forces.

Again in analogy with MD, in a DPD run the time evolution of the position ($\boldsymbol{r}_i(t)$) and momentum ($\boldsymbol{p}_i(t)$) of each particle is governed by Newton's equations:

$$\frac{\mathrm{d}\boldsymbol{r}_i}{\mathrm{d}t} = \frac{\boldsymbol{p}_i(t)}{m_i} \quad \frac{\mathrm{d}\boldsymbol{p}_i}{\mathrm{d}t} = \boldsymbol{f}_i(t) \tag{6}$$

where m_i, and $\boldsymbol{f}_i$ are the mass and total force, respectively, of particle i.

A force exerted on a particle i by a particle j, $\boldsymbol{F}_{ij}$, contains three components, each of which is pairwise additive and lies along the lines connecting the centers of particles i and j: a conservative ($\boldsymbol{F}_{ij}^{\mathrm{C}}$), a dissipative ($\boldsymbol{F}_{ij}^{\mathrm{D}}$), and a random ($\boldsymbol{F}_{ij}^{\mathrm{R}}$) force. Accordingly, the total force $\boldsymbol{f}_i$ acting on a particle i is given by:

$$\boldsymbol{f}_i = \sum_{i \neq j} \boldsymbol{F}_{ij} = \sum_{i \neq j} \boldsymbol{F}_{ij}^{\mathrm{C}} + \boldsymbol{F}_{ij}^{\mathrm{D}} + \boldsymbol{F}_{ij}^{\mathrm{R}} \tag{7}$$

$\boldsymbol{F}_{ij}^{\mathrm{C}} = a_{ij} w^{\mathrm{C}}(r_{ij}) \boldsymbol{e}_{ij}$ represents a purely repulsive conservative force, $\boldsymbol{F}_{ij}^{\mathrm{D}} = -\gamma w^{\mathrm{D}}(r_{ij})[\boldsymbol{v}_{ij}\boldsymbol{e}_{ij}]\boldsymbol{e}_{ij}$ slows down the particle motions with respect to each other, thus accounting for the effects of viscosity, and $\boldsymbol{F}_{ij}^{\mathrm{R}} = \sigma w^{\mathrm{R}}(r_{ij})(\theta_{ij}/\sqrt{\Delta t})\boldsymbol{e}_{ij}$ provides the thermal or vibrational energy of the system. Here, a_{ij} is the maximum repulsion between particles i and j, $\boldsymbol{e}_{ij} = \boldsymbol{r}_{ij}/r_{ij}$, $\boldsymbol{r}_{ij} = \boldsymbol{r}_i - \boldsymbol{r}_j$, $r_{ij} = |r_i - r_j|$, $\boldsymbol{v}_{ij} = (\boldsymbol{v}_i - \boldsymbol{v}_j)$, $v_i = p_i/m_i$, w^{C}, w^{D} and w^{R} are, respectively, the conservative, dissipative, and random weight functions, γ and σ are the coefficients of the dissipative and random forces, respectively, Δt is the time step, and θ_{ij} is a Gaussian random number with zero mean and unit variance ($\theta_{ij} = \theta_{ji}$).

All of the above forces are acting within a sphere of interaction or *cut-off radius* r_c, which practically constitutes the only length scale in the entire system. In addition, the fluctuation-dissipation theorem[11] requires:

$$w^{\mathrm{D}}(r) = [w^{\mathrm{R}}(r)]^2\sigma^2 = 2\gamma k_{\mathrm{B}}T \tag{8}$$

where k_{B} is the Boltzmann constant and T the system temperature. The conservative force weight function is given by $w^{\mathrm{C}}(r_{ij}) = 1 - (r_{ij}/r_{\mathrm{c}})$ in which $r_{ij} < r_{\mathrm{c}}$ and is zero otherwise. The dissipative and random weight functions take the general form:[12]

$$w^{\mathrm{D}}(r_{ij}) = \left[w^{\mathrm{R}}(r_{ij})\right]^2 \begin{cases} \left(1 - \dfrac{r_{ij}}{r_{\mathrm{c}}}\right)^2 & r_{ij} < r_{\mathrm{c}} \\ 0 & r_{ij} \geq r_{\mathrm{c}} \end{cases} \tag{9}$$

Finally, when modeling polymers, another force is active in the system, *i.e.*, the harmonic spring connecting the adjacent particles i and j:

$$\boldsymbol{F}_{ij}^{\mathrm{spring}} = -K(\boldsymbol{r}_{ij} - \boldsymbol{r}_0)\boldsymbol{e}_{ij} \tag{10}$$

where K is a spring constant and r_0 is the equilibrium distance between two adjacent particles.

DPD modeling for copolymer and nanoparticle. The copolymer considered in this work is constituted by poly(styrene)–poly(vinylpyridine) (PS-PVP) blocks. The molecular weight of the PS-PVP copolymer is approximately 14600 Da. The macromolecule is described by a flexible chain model, which is constituted of soft particles connected through harmonic springs, where each spherical bead represented a segment with a statistical distribution of the PS-PVP copolymer. In our previous paper,[13] we have shown that the characteristic ratio gives reliable results in describing the poly(styrene)–poly(vinylpyridine) system. Here, we employed the same statistical level approach for mapping the molecular structure of the copolymer into a flexible chain. The number of beads in each statistical unit was determined using the molecular mass of each block copolymer, molar mass of the repeat unit, degree of polymerization, and the characteristic ratio C_∞ of each polymeric block. A detailed description of the structural properties and the mapping of the atomistic structures to a mesoscale model is given in ref. 4. Following the proposed procedure, the PS-PVP copolymer is represented by a $\mathrm{PS}_n\mathrm{PVP}_m$ spring-bead chain, of total length of $N_{\text{PS-PVP}} = n + m = 14$. Bead of type PS represent poly(styrene), and bead of type PVP poly(*b*-2-vinylpyridine).

Each DPD gold nanoparticle is modeled by an icosahedral structure, devised as being constituted by a central DPD bead, connected to 12 other DPD beads on each vertex of the icosahedrons (Fig. 7).

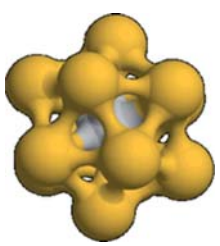

Fig. 7 Geometry and definition of the icosahedral nanoparticles considered in this work: a central core DPD bead (white) surrounded by another 12 DPD beads of type PS or Au (yellow) (depending on the coverage type considered), one on each vertex of the icosahedron.

Nanoparticle shape was preserved by employing a high value of the spring constant (*i.e.* $K = 200$), whilst a value of the spring constant of 4 was used for the polymer chain. The radius of the icosahedron was set equal to $R_{int} = 0.72r_c$ ($r_c = 16.8$ Å); the equilibrium distance for the bond spring between the surface beads was fixed to $r_0 = 0.76r_c$, that for the bond spring between the central and surface beads was equal to $r_0 = 0.72r_c$, and an equilibrium value of $r_0 = 0$ was employed for the polymer bonds.

In order to evaluate the effect of nanoparticle concentration on the morphology of the composite, three different nanoparticle volume fraction ϕ_p were considered: 0.05, 0.1 and 0.2. The effect of a different coverage of the nanoparticle by one of the two blocks, *i.e.*, PS, was mimicked by considering the following icosahedral particle architectures: PS_1Au_{12}, PS_2Au_{11}, PS_3Au_{10} and PS_4Au_9. According to this notation, for instance, PS_1Au_{12} identifies a nanoparticle coverage in which one bead on the icosahedron vertices is of type PS and the remaining twelve are of type Au, where Au identifies a bead representing Au atoms.

Interaction parameters. Having set the coarse-grained model of each component, the following step is the determination of the DPD interaction parameters a_{ij}. This quantity accounts for the underlying chemistry of the system considered and expresses the intra- and inter molecular interactions between DPD particles. There is a close relationship between the soft repulsive sphere model employed in DPD and the well-known Flory–Huggins model for polymer interactions. This relationship allows us to translate the repulsion parameters a_{ij} into the more familiar Flory–Huggins interaction parameter χ_{ij}.[14] In this work we applied the following relationship, as proposed by Glotzer and her group:[15]

$$a_{ij} = a_{ii} + 3.27\left(1 + \frac{3.9}{N_{AB}^{0.51}}\right)\chi_{ij} \quad (11)$$

where N_{AB} is the total chain length of the mesoscale model of a generic AB copolymer. Following the procedure described in our previous work,[13] we assumed a Flory–Huggins interaction parameter corresponding to $\chi_{PS\text{-}PVP} = 2.057$. According to eqn (11), for a mesoscopic chain of total length $N_{PS\text{-}PVP} = 14$, the related DPD interaction parameter is $a_{PS\text{-}PVP} = 38.56$.

In contrast to pure diblock copolymer systems, where mesoscopic mapping stems directly from the correspondence between DPD and Flory–Huggins type polymer models and solubility parameters, the mapping of solid particles-diblock interactions is not a straightforward task. In this work we pursued to obtain the solid–polymer mesoscopic interaction parameters a_{ij} from the relevant binding energies retrieved from molecular dynamics calculation, adapting a well-validated approach from our group.[16]

Atomistic models. As far as the Au molecular model is concerned, starting from relevant crystallographic coordinates,[17] we built the unit cell using the *Crystal Builder* module of *Materials Studio* (v.5.0, Accelrys, San Diego, USA). With the aim of estimating the interaction energies between all system elements accurately, and since these quantities are highly sensitive to the non-bonded components of the force field (FF) employed, we decided to adopt here an *ad hoc* modified *Compass* FF, developed recently by Heinz and co-workers.[18] As demonstrated by the authors, this accurately derived FF is able to describe the interfacial thermodynamics properties with a deviation from experiment amounting only to 10% in comparison to 100% with earlier models, which constitutes a fundamental step toward quantitative modeling of sensitive interfacial processes involving metal surfaces.

Accordingly, the resulting lattice of our Au model is face centered cubic (fcc) and characterized by the following lattice parameters: $a = b = c = 4.0785$ Å, and $\alpha = \beta = \gamma = 90°$, in excellent agreement with the model validated by Heinz.[18] Supercells of approximately $2 \times 2 \times 0.8$ nm^3 size ($5 \times 5 \times 2$ unit cells) were employed in all MD simulations.

Both PVP and PS model chains were created as follows: each polymer constitutive unit was firstly built and optimized again using the *Compass* FF, and then polymerized to the desired degree of polymerization. In order to obtain a reasonable sampling of the polymer conformational space, we built 10 different configurations of three PVP and PS chains, using the *Amorphous Builder* module of *Materials Studio*, which employs a version of the *Rotationa Isomeric State* (*RIS*) method[19] for generating polymer chain configurations. Each polymeric structure was then relaxed and subjected to a combined molecular mechanics/molecular dynamics simulated annealing (MDSA) protocol.[20]

Atomistic MD simulations. Resorting to atomistic MD simulations in the constant volume–constant temperature (*NVT*) ensemble allows the retrieval of important information on the interaction and binding energy values between the different components of a polymer–particle nanocomposite system.[16a,16c,21] In the present case, the technique basically consists in simulating the interface between the gold surface and the copolymer by building a cell that is "stretched" along the *c*-direction (up to 150 Å); in this way, even if the model is still 3D periodic, there are no interactions between the periodic images in the *c* direction, ultimately resulting in a pseudo-2D periodic system,[22] from which the interaction energies and, ultimately, the binding energies between all system components can be calculated (*vide infra*).

According to our approach, we created a cell of 150 Å in height and copied each of the 10 configurations of PVP or PS in 10 identical cells, thus obtaining 10 different model systems for each single polymer system (*i.e.*, 20 systems in total). The *NVT* MD runs were performed with *Materials Studio Discover* module. Each simulation was run at 298.15 K for 500 ps, applying the Ewald summation method[23] for treating Coulomb interactions; an integration step of 1 fs, and adopting the Nosé thermostat (Q ratio = 1) were also adopted. The energetic analysis was conducted on the equilibrated portion of the MD trajectory, and all energy values were averaged over the 10 configurations for each polymer.

The underlaying procedure used to calculate the interaction energies and, hence, the binding energy values E_{bind} between all system components, is well established.[20] For the binding energy E_{bind} calculations, we started from the concept that the binding energy of a system composed, for instance, of poly(styrene) (PS) and gold (Au), may be calculated from the following equation

$$E_{bind}^{PS\text{–}Au} = E_{PS} + E_{Au} - E_{PS\text{–}Au} \quad (12)$$

Table 2 DPD bead–bead interaction parameters used in this work

a_{ij}	PS	PVP	Au
PS	25.00		
PVP	38.56	24.11	
Au	29.76	26.23	23.00

where the first two terms represent the energy of poly(styrene) and gold, consisting of both valence and nonbonded energy terms, and the last term is the interaction energy between the two components, made up of nonbonded terms only. By definition, the binding energy E_{bind} is the negative of interaction energy. Thus, from each trajectory frame of the system, we began by deleting the PS molecules, leaving the gold surface alone, and thus calculated the energy of the slab (E_{Au}). Similarly, we next deleted the metal layer from the PS-Au system, and calculated E_{PS}. The remaining binding energy E_{bind}(PVP/Au) is computed in an utterly analogous fashion from the corresponding energy components.

Atomistic-DPD mapping. For the calculation of the DPD interaction parameters a_{ij} we adapted the recipe described in ref. 16 to the present system. Thus, we set the bead–bead interaction parameter for poly(styrene)–poly (styrene) interaction equal to $a_{PS-PS} = 25.00$, according to an appropriate value for a density value of $\rho = 3$.[14] The gold–gold interaction parameter was set to a lower value (*i.e.* $a_{Au-Au} = 23.00$), in order to mimic the aggregation tendency between bare nanoparticles. Once these two parameters were set, and their values associate with the corresponding values of the self and mixed rescaled DPD energies, all the remaining bead–bead interaction parameter for the DPD simulation could be easily obtained, starting from the atomistic binding energies as described in detail in our previous papers.[16] The entire set of mesoscale interaction parameters employed in this work is summarized in Table 2.

It is known from literature[24,25] that the nitrogen lone-pair electrons in the aromatic rings of PVP favorably interact with the Au atoms of the nanoparticle, resulting in an attractive interaction. This tendency is accounted for by a lower value of the mesoscale interaction parameter a_{PVP-Au} with respect to a_{PS-Au}, as directly derived from lower scale atomistic simulations.

DPD simulation details. All simulations were performed in a cubic box of size $25.5r_c \times 25.5r_c \times 25.5r_c$. Periodic boundary conditions were applied. The cut-off radius r_c, the particle mass m_i, and k_BT are taken as units of length, mass and energy. More than 7–10 $\times$ 10^5 DPD steps were carried out in each DPD simulation using a time step of $\Delta t = 0.03$, depending on the system concerned. All simulations were performed with an in-house developed code.[26]

Acknowledgements

Z. P. and M. L. acknowledge support by the Grant Agency of the Czech Republic (Grant No. 203/08/0094), by the Grant Programme of the Academy of Sciences of the Czech Republic "Nanotechnology for Society" (Project No. KAN400720701), by the Internal Grant Agency of the J. E. Purkinje University (Grants No. 53224 15 0008 01 and No. 53222 15 0006 01), and by the European Community under the 7th Framework Programme (Project COST TD0802/OC10053).

Notes and references

1 W. J. Work, K. Horie, M. Hess and R. F. T. Stepto, *Pure Appl. Chem.*, 2004, **76**, 1985–2007.
2 (*a*) *Polymer Nanocomposites: Synthesis, Characterization, and Modeling*, ed. R. Krishnamoorti and R. Vaia, ACS Symposium Series, American Chemical Society, Washington, DC, 2001; (*b*) *Polymer Nanocomposites*, ed. Y.-W. Mai and Z.-Z. Yu, CRC, Boca Raton, FL, 2006; (*c*) *Polymer Nanocomposites*, ed. K. Winey and R. Vaia, MRS Bulletin, Materials Research Society, Pittsburgh, PA, 2007; (*d*) R. Vaia and J. F. Maguire, *Chem. Mater.*, 2007, **19**, 2736–2751.
3 (*a*) A. Thomas, F. Goettmann and M. Antonietti, *Chem. Mater.*, 2008, **20**, 738–755; (*b*) A. B. R. Mayer, Encyclopedia of Materials: Science and Technology, Elsevier Science, Oxford, U.K., 2008, pp. 7449–7455; (*c*) P. K. Sudeep and T. Emrick, *ACS Nano*, 2009, **3**, 2870–2875; (*d*) C. K. Ober, S. Z. D. Cheng, P. T. Hammond, M. Muthukumar, E. Reichmanis, K. L. Wooley and T. P. Lodge, *Macromolecules*, 2009, **42**, 465–471; (*e*) H.-C. Kim, S.-M. Park and W. D. Hinsberg, *Chem. Rev.*, 2010, **110**, 146–177.
4 (*a*) J. J. Chiu, B. Kim, E. J. Kramer and D. J. Pine, *J. Am. Chem. Soc.*, 2005, **127**, 5036–5037; (*b*) B. J. Kim, J. Bang, C. J. Hawker, J. J. Chiu, D. J. Pine, S. Gyu Jang, S.-M. Yang and E. J. Kramer, *Langmuir*, 2007, **23**, 12693–12703.
5 Y.-T. Fu and H. Heinz, *Chem. Mater.*, 2010, **22**, 1595–1605.
6 (*a*) B. Hamdoun, D. Auserré, S. Joly, Y. Gallot, V. Cabuil and C. Clinard, *J. Phys. II*, 1996, **6**, 493–502; (*b*) B. Hamdoun, D. Auserré, S. V. Cabuil and S. Joly, *J. Phys. II*, 1996, **6**, 503–527; (*c*) J. Listak, I. F. Hakem, H. J. Ryu, S. Rangou, N. Politakos, K. Misichronis, A. Avgeropoulos and M. R. Bockstaller, *Macromolecules*, 2009, **42**, 5766–7773.
7 B. J. Kim, G. H. Fredrickson, J. Bang, C. J. Hawker and E. J. Kramer, *Macromolecules*, 2009, **42**, 6193–6201.
8 B. J. Kim, G. H. Fredrickson, C. J. Hawker and E. J. Kramer, *Langmuir*, 2007, **23**, 7804–7809.
9 A. J. Schultz, C. K. Hall and J. Genzer, *Macromolecules*, 2005, **38**, 3007–3016.
10 (*a*) P. J. Hoogerbrugge and J. M. V. A. Koelman, *Europhys. Lett.*, 1992, **19**, 155–160; (*b*) J. M. V. A. Koelman and P. J. Hoogerbrugge, *Europhys. Lett.*, 1993, **21**, 363–368.
11 P. Español and P. B. Warren, *Europhys. Lett.*, 1995, **30**, 191–196.
12 X. Fan, N.P.-T., S. Chen, X. Wu and T. Y. Ng, *Phys. Fluids*, 2006, **18**, 63102–63110.
13 M. Malý, P. Posocco, S. Pricl and M. Fermeglia, *Ind. Eng. Chem. Res.*, 2008, **47**, 5023–5038.
14 R. D. Groot and P. B. Warren, *J. Chem. Phys.*, 1997, **107**, 4423–4435.
15 M. A. Horsch, Z. Zhang, C. R. Iacovella and S. C. Glotzer, *J. Chem. Phys.*, 2004, **121**, 11455–11462.
16 (*a*) G. Scocchi, P. Posocco, A. Danani, S. Pricl and M. Fermeglia, *Fluid Phase Equilib.*, 2007, **261**, 366–374; (*b*) G. Scocchi, P. Posocco, M. Fermeglia and S. Pricl, *J. Phys. Chem. B*, 2007, **111**, 2143–2151; (*c*) G. Scocchi, P. Posocco, J.-W. Handgraaf, J. G. E. M. Fraaije, M. Fermeglia and S. Pricl, *Chem.–Eur. J.*, 2009, **15**, 7586–7592; (*d*) R. Toth, D.-J. Voorn, J.-W. Handgraaf, J. G. E. M. Fraaije, M. Fermeglia, S. Pricl and P. Posocco, *Macromolecules*, 2009, **42**, 8260–8270.
17 *CRC Handbook of Chemistry and Physics*, ed. D. R. Lide, CRC Press, Boca Raton, FL, 79th edn, 1998.
18 H. Heinz, R. A. Vaia, B. L. Farmer and R. R. Naik, *J. Phys. Chem. C*, 2008, **112**, 17281–17290.
19 N. D. Theodorou and U. W. Suter, *Macromolecules*, 1986, **19**, 139–154.
20 (*a*) M. Fermeglia, M. Ferrone and S. Pricl, *Fluid Phase Equilib.*, 2003, **212**, 315–329; (*b*) R. Toth, A. Coslanich, M. Ferrone, M. Fermeglia, S. Pricl, S. Miertus and E. Chiellini, *Polymer*, 2004, **45**, 8075–8083; (*c*) M. Fermeglia, M. Ferrone and S. Pricl, *Mol. Simul.*, 2004, **30**, 289–300.
21 (*a*) H. Kasemägi, A. Aabloo, M. K. Klintenberg and J. O. Thomas, *Solid State Ionics*, 2002, **147**, 367–375; (*b*) G. Tanaka and L. A. Goettler, *Polymer*, 2002, **43**, 541–553; (*c*) H. Kasemägi, A. Aabloo, M. K. Klintenberg and J. O. Thomas, *Solid State*

Ionics, 2004, **168**, 249–254; (*d*) F. Gardebien, J.-L. Bredas and R. Lazzaroni, *J. Phys. Chem. B*, 2005, **109**, 12287–12296; (*e*) D. R. Paul, Q. H. Zeng, A. B. Yu and G. Q. Lu, *J. Colloid Interface Sci.*, 2005, **292**, 462–468; (*f*) K. S. Katti, D. Sikdar, D. R. Katti, P. Ghosh and D. Verma, *Polymer*, 2006, **47**, 403–414.

22 S. Misra, P. D. III Femin and W. L. Mattice, *J. Comput.-Aided Mater. Des.*, 1995, **2**, 101–112.

23 P. P. Ewald, *Ann. Phys.*, 1921, **369**, 253–287.

24 (*a*) J. B. Kim, J. Bang, C. J. Hawker and E. J. Kramer, *Macromolecules*, 2006, **39**, 4108–4114; (*b*) J. B. Kim, G. H. Fredrickson and E. J. Kramer, *Macromolecules*, 2008, **41**, 436–447.

25 (*a*) M. S. Kunz, K. R. Shull and A. J. Kellock, *J. Colloid Interface Sci.*, 1993, **156**, 240–249; (*b*) R.-H. Ho, T. Lin, M.-R. Jhong, T.-M. Chung, B.-T. Ko and Y.-C. Chen, *Macromolecules*, 2005, **38**, 8607–8610.

26 (*a*) M. Lísal and J. K. Brennan, *Langmuir*, 2007, **23**, 4809–4818; (*b*) Z. Posel, M. Lísal and J. K. Brennan, *Fluid Phase Equilib.*, 2009, **283**, 38–48; (*c*) P. Petrus, M. Lísal and J. K. Brennan, *Langmuir*, 2010, **26**, 3695–3709.

